Atmos. Chem. Phys. Discuss., 10, 7699–7743, 2010
www.atmos-chem-phys-discuss.net/10/7699/2010/
© Author(s) 2010. This work is distributed under
the Creative Commons Attribution 3.0 License.

Atmospheric Chemistry and Physics Discussions

This discussion paper is/has been under review for the journal Atmospheric Chemistry and Physics (ACP). Please refer to the corresponding final paper in ACP if available.

African biomass burning plumes over the Atlantic: aircraft based measurements and implications for H_2SO_4 and HNO_3 mediated smoke particle activation

V. Fiedler[1,2], F. Arnold[1,2], S. Ludmann[2], A. Minikin[1], L. Pirjola[3,4], A. Dörnbrack[1], and H. Schlager[1]

[1]Deutsches Zentrum für Luft- und Raumfahrt, Institut für Physik der Atmosphäre, Oberpfaffenhofen, 82234 Wessling, Germany
[2]Max-Planck Institute for Nuclear Physics, (MPIK), Atmospheric Physics Division, P.O. Box 103980, 69029 Heidelberg, Germany
[3]Department of Physics, University of Helsinki, P.O. Box 64, 00014 Helsinki, Finland
[4]Department of Technology, Metropolia University of Applied Sciences, P.O. Box 4000, 00180 Helsinki, Finland

Received: 18 February 2010 – Accepted: 19 March 2010 – Published: 25 March 2010

Correspondence to: F. Arnold (frank.arnold@mpi-hd.mpg.de)

Published by Copernicus Publications on behalf of the European Geosciences Union.

Abstract

Airborne measurements of trace gases and aerosol particles have been made in two aged biomass burning (BB) plumes over the East Atlantic (Gulf of Guinea). The plumes originated from BB in the Southern Hemisphere African savanna belt. On the day of our measurements (13 August 2006), the plumes had ages of about 10 days and were respectively located in the middle troposphere (MT) at about 3000–5500 m altitude and in the upper troposphere (UT) at about 10 800–11 200 m. In the more polluted MT-plume, numerous measured trace species had markedly elevated abundances, particularly HNO_3 (5000–8000 pmol/mol), SO_2 (up to 1400 pmol/mol), and smoke particles with diameters larger than 250 nm (up to 2000 cm^{-3}). Our MT-plume measurements indicate that SO_2 released by BB had not experienced significant loss by deposition and cloud processes but rather had experienced OH-induced conversion to gas-phase sulfuric acid. By contrast, a large fraction of the released NO_x had experienced loss, most likely as HNO_3, by cloud processes and deposition. In the UT-plume, loss of NO_y and SO_2 by cloud processes and deposition was more pronounced compared to the MT-plume. Building on our measurements and accompanying model simulations, we have investigated trace gas transformations in the ageing and diluting plumes and their role in smoke particle processing and activation. Emphasis was placed upon the formation of sulfuric acid, nitric acid, and ammonium nitrate, and their influence on the activation potential of smoke particles. Our model simulations reveal that, after 13 August, the lower plume traveled across the Atlantic and descended to 1300 m and hereafter ascended again. During the travel across the Atlantic, the smoke particle mean diameter and sulfuric acid mass fraction increased sufficiently to allow the processed smoke particles to act as water vapor condensation nuclei already at very low water vapor supersaturations of only about 0.04%. Thereby, aged smoke particles had developed a potential to act as water vapor condensation nuclei in the formation of maritime clouds, including not only cumulus but even stratiform clouds.

ACPD

10, 7699–7743, 2010

1 Introduction

Biomass burning (BB) is a global phenomenon, which has an impact on the environment and climate (Crutzen et al., 1979; Andreae, 1983; Crutzen and Andreae, 1990; Houghton et al., 2001). BB plumes contain elevated concentrations of pollutants, including smoke particles and primary as well as secondary combustion gases. Savanna fires represent the single most important BB-type worldwide (Crutzen and Andreae, 1990; Andreae, 1991; Koppmann et al., 2005). Africa contains about two thirds of the worlds savanna regions and 90% of the African savanna fires are believed to be human induced (Koppmann et al., 2005). Since BB plumes can be transported over thousands of kilometers, their impact on the environment and climate may occur far away from BB regions. For example, elevated O_3 present over the South Atlantic has been attributed to secondary O_3 formation in BB plumes originating from Africa (see review by Koppmann et al., 2005; Real et al., 2009).

BB releases primary pyrogenic gases (Koppmann et al., 2005) and primary smoke particles (see recent review by Reid et al., 2005) whose characteristics and relative emission rates depend on various factors including particularly the type of bio material combusted and the burning conditions (flaming, smoldering). Primary pyrogenic gases include, besides the major combustion products H_2O and CO_2, numerous minor gases, particularly CO, hydrocarbons, NO and SO_2 (cf. Andreae and Merlet, 2001). Interaction of NO and organics leads to the formation of secondary ozone, which represents a greenhouse gas, an important atmospheric oxidant, and a precursor of OH radicals.

Primary pyrogenic particles contain solid cores (mostly soot (elemental carbon=EC) and ash) and a semi-volatile coating composed of low vapor pressure organics (organic carbon=OC), which is formed by rapid OC-condensation. The resulting internally mixed smoke particles have initial median diameters of about 125 nm and a mass ratio OC/EC of about 5–10 (Reid et al., 2005).

As a BB burning plume ages and dilutes, chemical transformations of primary pyrogenic gases take place leading to secondary gases including particularly O_3. Some

ACPD
10, 7699–7743, 2010

secondary gases undergo gas-to-particle conversion leading to chemical processing and additional size growth of primary smoke particles. Of these secondary gases, sulfuric acid (H_2SO_4) and nitric acid (HNO_3) are particularly important. Sulfuric acid is formed by OH-induced conversion of the primary pyrogenic gas SO_2 (cf. Reiner and Arnold, 1993, 1994). Nitric acid is formed via OH-induced conversion of NO_2, which results from rapid conversion of primary pyrogenic NO. Due to its very low saturation vapor pressure, sulfuric acid condenses on smoke particles and, due to its very large hygroscopicity, tends to increase smoke particle-hygroscopicity. Nitric acid has a much higher saturation vapor pressure than sulfuric acid and, in most atmospheric conditions, does not condense on smoke particles. However, HNO_3 may react with gases possessing large proton affinities. A key candidate is the primary pyrogenic trace gas ammonia (NH_3). Its reaction with HNO_3 ultimately leads to condensed-phase ammonium nitrate (NH_4NO_3), which is thermally stable at most temperatures encountered in the free troposphere. Nitric acid may also react with ammonium salts already contained in smoke particles leading to condensed-phase NH_4NO_3. Thereby acids become displaced, which may leave the smoke particle.

However, smoke particles as well as the gases HNO_3, NH_3 and SO_2, the precursor of H_2SO_4, may experience substantial loss by cloud-processes and deposition. Therefore, their concentrations in an aged BMB plume and the effects on smoke particle processing by H_2SO_4 and HNO_3 are difficult to predict. Due to their large solubilities in water, the gases HNO_3 and NH_3 are potentially strongly affected by removal via cloud processes and deposition (Seinfeld and Pandis, 1998). By contrast, SO_2 has a much lower solubility, but dissolved SO_2 may undergo liquid-phase conversion to sulfate, which will remain in the condensed-phase.

Considering relevant emission factors and their uncertainty ranges (Table 1) for primary smoke particles and SO_2, one finds that the ultimate H_2SO_4-mass fraction of smoke particles may on average be about 0.065 and range between about 0.025 and 0.15. However, this applies only if all SO_2 would undergo conversion to H_2SO_4 and if both SO_2 and primary particles would not experience loss by cloud-processes and

deposition.

Sulfuric acid, due to its large hygroscopicity, may have a particularly large effect on the ability of smoke particles to take up water molecules from the gas-phase in conditions with relative humidity RH<100%, and to act as water vapor condensation nuclei (CCN=cloud condensation nuclei) in cloud formation, in conditions with RH>100%. Smoke particle processing by H_2SO_4 and NH_4NO_3 is particularly important for atmospheric conditions with only small water vapor supersaturations WSS of only about 0.05%, which are typical for the maritime boundary layer and for maritime stratiform cloud formation (Seinfeld and Pandis, 1998). The larger the H_2SO_4 mass fraction of a smoke particle, the smaller will be the activation water vapor supersaturation (WSSa) required for activation. The H_2SO_4 formed in the ageing plume increases with time until precursor SO_2 is exhausted. Therefore, also the H_2SO_4 mass fraction of smoke particles increases with time. As a consequence, the ability of a smoke particle of a given size to act as CCN (at a given water vapor supersaturation) increases with time as the H_2SO_4 mass fraction increases due to H_2SO_4 uptake. In addition, coagulation contributes to increase the smoke particle diameter, which also contributes to decrease the water vapor supersaturation required for activation. However as the plume ages, the number concentration of smoke particles decreases strongly, due to coagulation and plume dilution. Therefore, the number concentration of smoke particles which can be activated, at a given WSS, is expected to have a maximum at a certain plume age. The larger the rate of SO_2-conversion to H_2SO_4, the smaller will be the plume age at which this maximum occurs and the larger will be the maximum concentration of smoke particles which can be activated.

Therefore, the rate of SO_2 conversion to gas-phase H_2SO_4 in the ageing and diluting plume is crucial in determining the H_2SO_4 mass fraction of smoke particles, and thereby the evolution of their activation potential. This rate is determined by the OH concentration and its time variation in the plume. In a BB plume, the OH concentration is thought to be controlled mostly by OH-loss via the reaction of OH with NO_2 leading to HNO_3 and by OH-formation via processes involving organic plume gases (preferably

acetone-photolysis leading to about 3.2 HO_x radicals per acetone molecule) (Singh et al., 1994; Folkins et al., 1997). While elevated NO_x tends to decrease OH, increased acetone tends to increase OH. Previous measurements of OH in an aged BB plume at 9000–1000 m altitude have indicated OH concentrations of about 0.1 pmol/mol (Folkins et al., 1997). These, were not much different from ambient OH concentrations outside the BB plume. This led to the conclusion that the additional NO_x-induced OH loss was approximately offset by an additional acetone-induced OH formation.

The present paper reports on airborne measurements of HNO_3 and SO_2 along with other gases and smoke particles in two aged savanna fire plumes over the East Atlantic, off the west coast of equatorial Africa (Gulf of Guinea). At the time of our measurements one plume was located in the middle troposphere (MT) and one in the upper troposphere (UT). From the trace gas data we infer the formation of H_2SO_4, HNO_3 and NH_4NO_3 in the plumes and discuss implications with regard to their influence on the smoke particle activation potential.

2 Experiment

Our airborne BB plume measurements were part of the AMMA (African Monsoon Multidisciplinary Analyses) campaign and took place on 13 August 2006, off the western coast of Tropical Africa (Ghana). The measurements were made by various instruments on board the DLR (Deutsches Zentrum für Luft- und Raumfahrt, Oberpfaffenhofen) research aircraft Falcon, when it dived into and cruised in the plume at altitudes between about 3900 and 5500 m.

The AMMA project aims at a better understanding of the West African Monsoon, its influence on the processing of chemical emissions and its associated regional-scale and vertical transports. For this purpose an airborne campaign was conducted in July/August 2006 with special interest on biomass burning emissions. Further objectives were the characterization of the impact of mesoscale convective systems on the ozone budget in the upper troposphere and the evolution of the chemical compo-

CC BY

sition of these convective plumes as they move westward toward the Atlantic Ocean. Another objective was to discriminate the impact of remote sources of pollution over West Africa, including transport from the middle East, Europe, Asia and from southern hemispheric BB fires.

Sulfur dioxide (SO_2) was measured by a chemical ionization mass spectrometry (CIMS) method with permanent in-flight calibration using isotopically labeled SO_2. The CIMS-instrument, which has been developed by MPI-K (Max-Planck-Institute for Nuclear Physics, Heidelberg) in collaboration with DLR, is equipped with a powerful ion trap mass spectrometer. A comprehensive description of the measurement system can be found in Speidel et al. (2007); Fiedler et al. (2009b,a). The method is based on gas-phase ion molecule reactions in a flow reactor. These reactions involve reagent ions CO_3^- which react with atmospheric SO_2 ultimately leading to SO_5^- product ions. By measuring the abundance ratio of product and reagent ions with the ion trap mass spectrometer, the SO_2 mole fraction can be determined. The SO_2 measurements have a time resolution of 1 s and a detection limit (2 sigma level) of about 20 pmol/mol. The relative error is about plus or minus 12% for SO_2 mole fractions larger than 100 pmol/mol and increases close to the detection limit to plus or minus 40% (Speidel et al., 2007).

Nitric acid (HNO_3) measurements have been carried out with the same CIMS instrument. Principally, HNO_3 can be detected using the gas-phase ion molecule reaction of CO_3^- with HNO_3. This reaction leads to $(CO_3HNO_3)^-$ cluster ions, which again are detected by the mass spectrometer.

Simultaneous measurements of other trace gases (CO_2, CO, NO, NO_y, H_2CO, O_3) were carried out on the Falcon by DLR (see Table 2).

Carbon monoxide (CO) was detected using vacuum resonance fluorescence in the fourth positive band of CO (Gerbig et al., 1999). The accuracy of the CO measurements is ±10% for a time resolution of 5 s and with a detection limit of 3 nmol/mol. Carbon dioxide (CO_2) was measured with a differential nondispersive infrared instrument (NDIR), the detection limit was 0.1 µmol/mol, the sampling rate 1 s and the accuracy

ACPD
10, 7699–7743, 2010

±0.1% (Schulte et al., 1997).

Nitric oxide (NO) and the sum of reactive nitrogen compounds (NO_y) were measured using a chemiluminescence technique (Schlager et al., 1997; Ziereis et al., 2000). The NO_y compounds are catalytically reduced to NO on the surface of a heated gold converter with addition of CO. The accuracy of the NO and NO_y measurements is ±8% and ±15%, respectively. The time resolution is 1 s and the detection limit 5 pmol/mol and 15 pmol/mol, respectively.

Ozone (O_3) was measured using an UV absorption photometer (Schlager et al., 1997; Schulte et al., 1997). The accuracy of the ozone detection is ±5%, the detection limit is 1 nmol/mol and the time resolution 4 s. Formaldehyde HCOH has been measured using a Hantzsch reaction instrument (Kormann et al., 2003). The detection limit of this instrument is 84 pmol/mol, the time resolution is 180 s and the uncertainty ±30% at a mixing ratio of 300 pmol/mol. Table 2 compiles the measured atmospheric substances, measurement techniques, and specifications of the techniques.

3 Plume localization and trajectories

Figure 1a, b shows a MODIS (Moderate Resolution Imaging Spectroradiometer) satellite image of fires in Africa for the period 1–10 August 2006. MODIS detects hotspots/fires as a thermal anomaly using data from the middle infrared and thermal infrared bands. In most cases, this thermal anomaly is a fire, but sometimes it is a volcanic eruption or the flare from a gas well. The minimum detectable fire size is a function of many different variables (scan angle, sun position, land surface temperature, cloud cover, amount of smoke and wind direction etc.), so the precise value slightly varies with these conditions. Results of validation measurements indicate that the minimum flaming fire size typically detectable at 50% probability with MODIS is on the order of 100 m^2. Under ideal conditions performance is somewhat better and the smallest detectable fire size is approximately 50 m^2. As can be seen from the figure, fires had been active in a large region covering the Southern Hemisphere African con-

tinent mostly south of the tropical rainforest belt, which suggests that most of the fires were savanna fires. The core of the BB region with the largest density of fire spots was located between about 20–30 deg east and 5–15 deg south.

Figure 2 shows an image of light absorbing aerosol particles measured on 13 August (day of our airborne measurements) by OMI (ozone monitoring instrument) aboard the AURA satellite. Plotted is the aerosol index AI (measures how much the backscattered UV wavelength of a polluted atmosphere differs from that of a pure atmosphere (a positive AI values means absorbing aerosols). The OMI instrument can distinguish between aerosol types, such as smoke, dust and sulfates, and measures cloud pressure and coverage, which provide data to derive tropospheric ozone. The instrument employs hyperspectral imaging to observe solar backscatter radiation in the visible and ultraviolet. The instrument is a contribution of the Netherlands's Agency for Aerospace Programs (NIVR) in collaboration with the Finnish Meteorological Institute (FMI) to the Earth Observing System (EOS) Aura mission. The AI image (Fig. 2) reveals the presence of an extended pollution plume rich in light absorbing aerosol particles, mostly soot particles. The plume of light absorbing particles is present preferably over the Tropical East Atlantic and also over Tropical Africa and covers an area of at least 4 million km^2. Unfortunately, the height of the soot plume cannot be obtained from the satellite image. The plume exhibits a horizontally inhomogeneous distribution and the dive of the Falcon into the plume took place in one of the denser plume regions (dive region is marked by a cross in Fig. 2).

CALIPSO (**C**loud **A**erosol **L**idar and **I**nfrared **P**athfinder **S**atellite **O**bservations, see also http://www.nasa.gov/calipso) lidar data also confirm the presence of the middle troposphere plume (hereafter MT-plume) over the Gulf of Guinea, on 13 August. For the region of the Falcon dive into the MT-plume, they indicate a top altitude of about 5000 m and a bottom altitude of about 3000 m (cf. Real et al., 2009).

Figure 3 shows the Falcon-flight path projected on the map with the flight altitude color coded. To probe the plume, the Falcon took off on 13 August 2006 at Ouagadougou (Burkina Faso) and flew at 9000–11 000 m altitude in southern direction to

CC BY

the equatorial Atlantic region off the coast of Ghana (western branch of the flight path in the Figure). Here it dived into the plume to a lowest height of 3900 m where it cruised for about 5 min. Hereafter it climbed out of the plume again and flew back to Ouagadougou (right branch in the Figure).

Figures 4a, b show two photographs of the MT-plume, taken by one of the authors aboard the Falcon. One photograph was taken at 5500 m altitude (a) just before diving into the plume. Here the MT-plume defined the horizon. The sky close to the horizon was already whitish and only well above the horizon became deep blue. When looking downward at an angle of about 45 degrees, features at the planetary surface are hardly visible, indicating severe visibility degradation. The other photograph was taken, when cruising at 3900 m altitude in the plume (b). Here severe horizontal visibility degradation is noticeable, not allowing to see the horizon. When looking downward at an angle of about 45 degrees, surface features seem to be better visible compared to looking from 5500 m altitude.

To investigate the origin of the MT-plume, we have made back-trajectory simulations using the LAGRANTO model (Wernli and Davies, 1997). Figure 5 shows a typical 10-day back-trajectory of the lower plume superimposed on a map. The altitude of the trajectory is indicated by the color code. The time span between tick-marks (filled circles) is 24 h. Also shown on the map are the core of the fire region as detected by MODIS between 1 and 10 August 2006 (red dots) and the African copper belt region (blue dots). The so-called African copper belt is the region in Zaire and Zambia, where major copper smelters are located, which represent major SO_2 sources.

On 4 August, 10 days prior to our measurements, the air parcel which on 13 August was intercepted by the Falcon at 3900 m, passed at about 1200 m altitude over the core of the fire region, about 500 km west of the copper-smelters. Hereafter, during 7–10 August, the air parcel traveled at about 4000 m altitude over the north western region of the fire belt. Hence, it seems that the air parcel took up pyrogenic gases preferably during 4 August when it passed at low altitudes over the core of the fire belt. This would imply a time span of 10 days for transit from the core of the BB region to the

ACPD
10, 7699–7743, 2010

measurement region. Uptake of copper smelter SO_2 is less likely since the smelters are located about 500 km east of the trajectory. On 5 August, while leaving the core of the BB region, the air parcel ascended from about 1200 m to about 3000 m and on 8 August it reached about 4000 m altitude.

To investigate the fate of the MT-plume, after 13 August, we have made LAGRANTO forward-trajectory model simulations. Figure 6 shows a combination of the 10-day back-trajectory with a 10-day forward simulation of the trajectory, starting on 13 August at 3900 m altitude at 12:00 UTC. It indicates that, after our measurements, the plume parcel traveled westward over the Atlantic and reached the coast of northern Brazil on 20 August. Hereafter it traveled northwards over the Atlantic Ocean again. While traveling over the Atlantic, the plume parcel descended to a lowest height of about 1300 m altitude.

4 Measured species

Figure 7a shows time series of flight altitude and the measured SO_2 mole fraction measured by the CIMS-instrument. As the Falcon dived from 9000 to 5500 m, SO_2 increased slightly from about 30 and 40 pmol/mol. After a short cruise just above the top of the visible plume at 5500 m, the Falcon dived further to 3900 m. During that dive, between 5500 m to about 5000 m, SO_2 increased abruptly by a factor of about 10 to about 400 nmol/mol, and below about 5250 m, SO_2 further increased abruptly to 1400 pmol/mol. During the following short cruise at 3900 m, SO_2 varied between 1400 and 1250 pmol/mol. After that 5 min cruise at 3900 m, as the Falcon ascended, SO_2 decreased abruptly to 430 pmol/mol, and above 4700 m, SO_2 decreased further to the previous atmospheric background value of 30–40 pmol/mol, reached at 5700 m. The altitude profile of the SO_2 mole fraction (Fig. 7b indicates the presence of a plume in the MT (hereafter termed MT plume) with a sharp top at about 5200 m(descent)–5000 m(ascent) and two altitude regimes with different degrees of SO_2 pollution, including an upper plume regime and a main plume regime (below about 4200 m). The

ACPD
10, 7699–7743, 2010

Falcon has spent about 11 minutes inside the MT- plume, below 5200 m, corresponding to a horizontal distance of about 100 km. On that horizontal length scale the top altitude of the MT plume was quite similar, differing only by 200 m.

As the Falcon ascended further, a pronounced local SO_2 maximum of about 90 pmol/mol was observed at 12:24 UTC (Fig. 7a, b ,about 11 000 m altitude). This indicates the presence of a second much less polluted plume the UT at about 10 800–11 200 m altitude (hereafter termed UT-plume). Its height extension was only about 400 m which is much less than that of the MT-plume (about 2500 m).

Figure 8 shows the altitude profiles of SO_2, H_2O, temperature, and relative humidity (RH). In the MT-plume, H_2O and RH are elevated, The absolute water vapor mole fraction reaches up to 7200 µmol/mol, in the upper part of the MT-plume in a layer between about 4400 and 5100 m. This indicates upward transport of humid air. Temperature reached up to 292 K at about 4000 m and RH reached up to 64%, in the upper part of the MT-plume, at 5000 m.

Figure 9a shows the same as Fig. 7a but includes also the other measured trace gases (given is CO_2 and dCO_2, NO_y, NO, HNO_3, and HCOH). Figure 9b shows the corresponding altitude profiles of measured trace gases and particles.

The shape of the altitude profile of NO_y is similar to SO_2, clearly showing increases in the MT-plume. At 3900 m, NO_y reaches up to about 8 nmol/mol and the mole fraction ratio dNO_y/dCO_2 is about 6×10^{-4} (see Table 1). In the MT-plume at 3900 m, NO_x/NO_y is only 0.13 whereas the measured HNO_3/NO_y ranges between about 0.63 and 1.1. The trace gases CO, HCOH and O_3 are markedly increased in the MT-plume. The mole fraction ratio dCO/dCO_2, measured in the MT-plume at 3900 m is 0.043. The mole fraction ratio $dHCOH/dCO_2$ measured in the MT-plume at 3900 m is 7.7×10^{-5}.

The trace gas HCOH can be a primary pyrogenic gas and a secondary gas formed in the plume from primary gases. The gas O_3 represents a secondary gas formed in the plume via NO-oxidation by organics. For example, reaction of NO with the PA-radical (peroxyacetyl radical) leads to NO_2. Photolysis of NO liberates O which combines with O_2 to form O_3.

ACPD
10, 7699–7743, 2010

Figure 10 shows, for the MT-plume interception, time sequences of number concentrations N(170–300) and N(300–1100) of aerosol particles possessing diameters between 170 and 300 nm and 300 than 1100 nm. Also given are time sequences of the SO_2 mole fraction and the flight altitude of the Falcon. As the Falcon dives into the MT-plume both aerosol particle concentrations increase very steeply and are correlated with SO_2. Pronounced maxima of particle concentrations were observed at 4–5 km altitude, just shortly before the Falcon had dived to the lowest altitude of 3900 m. Particles possessing diameters 300–1100 nm were most abundant.

Altitude profiles of measured particle number concentrations along with the altitude profile of the SO_2 mole fraction are included in Fig. 9b. Plotted are concentrations of particles possessing diameters >4 nm, 250–900 nm, 650–3000 nm and 3000–20 000 nm. In addition particles with diameters larger than 4 nm, which have been heated to 250 °C during passage of the thermo-denuder, are plotted and denoted N4(nv). Hereafter, these particles will be termed "non-volatile (nv) particles". They contain black carbon and ash and perhaps also certain organic carbon species with very low vapor pressures.

The N4-altitude profile increases in the MT-plume with decreasing altitude, similar to SO_2. Above the MT-plume, N4 increases with increasing altitude and reaches maximum values of about 1300. In the MT-plume, N4(nv) is nearly identical to the total N4. This indicates that in the plume almost all particles contain non-volatile cores. Above the MT-plume, most particles do not contain non-volatile cores with d <4 nm.

The N250–900 are also very substantially increased (by a factor of up to about 1000) in the MT-plume and during dive are as large as the N4. This indicates that most particles had diameters larger than 250 nm. Of all measured trace substances, N250 exhibits the largest increase in the MT-plume, at 3900 m.

The N650–3000 profile also increases in the MT-plume (by a factor of up to about 5). The ratio N650–3000/N250–900 is only about 0.0001 at 3900 m altitude. By contrast to N250, N650 is nearly identical for the dive and climb. In comparison, primary smoke particles released from savanna fires have a median diameter of about 125 nm (Reid

ACPD
10, 7699–7743, 2010

et al., 2005).

N3000–20000 is very small (<0.01 cm^{-3}). This indicates that clouds were absent, which is consistent with the relatively low RH (<27%) in the MT-plume at 3900 m altitude (see Fig. 8).

Figure 11 shows three aerosol particle size distributions measured in and above the MT-plume at 7000, 4500, and in the MT-plume at 3900 m altitude. Above the MT-plume, the two distributions are very similar, both peaking at 20–30 nm. In the MT-plume at 3900 m, the size distribution is very different, peaking at about 300 nm. This indicates fewer small particles and many more large particles. The large particles are most likely aged smoke particles which are substantially larger than typical primary smoke particles (median diameter: about 125 nm, see above). The local minimum indicates that entrained background aerosol particles experienced removal via coagulation with smoke particles, since coagulation with smoke particles becomes more efficient for smaller particles.

The volume and mass concentrations of smoke particles can be inferred from the measured size distribution. Considering particles with diameters of up to 800 nm and assuming a specific weight of smoke particles of 1 g cm^{-3}, one obtains a smoke particle mass concentration of 6.5×10^{-11} g cm^{-3} (at 3900 m, 13 August, 12:04 UTC).

For SO_2, NO_y, H_2O, O_3, HCOH, N4, N4(nv) and N650 in the MT-plume downleg and uplegs of the altitude profiles are similar. By contrast, for CO, HNO_3, NO and N250 downleg and upleg data are markedly different. For CO, HNO_3 and NO, upleg data are larger. For N250, upleg data are lower.

These differences may be due to sampling line problems (wall-losses and memory effects). Particularly, for HNO_3, wall-losses may initially be large after the Falcon entered the HNO_3-rich plume. After sufficient HNO_3-coating of the sampling line wall, saturation may occur and gas-phase HNO_3 may pass the sampling line with a large probability (large sampling line transmission). By contrast to HNO_3, NO_y (which is mostly HNO_3) may not be affected by severe sampling line losses since in the NO_y instrument HNO_3 is rapidly converted to NO and therefore does not have to pass through

ACPD
10, 7699–7743, 2010

a long sampling line. However, CO and NO exhibit behaviors similar to HNO_3 although these gases are much less sticky than HNO_3, and therefore should not be affected by severe wall-losses.

Therefore, alternative processes may also be considered as an explanation. Concerning HNO_3, a conceivable possibility may be HNO_3-recycling from aerosol-phase NH_4NO_3, preferably during climb. Generally, due to heat conduction from the cabin, the sampling line is at a higher temperature than the ambient atmosphere. The passage of cold atmospheric air through the sampling line cools the sampling line. As atmospheric temperature increased with decreasing altitude (Fig. 8), the cooling decreased during the dive. Therefore, the sampling line temperature increased during the dive. During the cruise at 3900 m, the sampling line temperature increased further. During the climb, cooling increased again and therefore the sampling line temperature decreased again, but was still larger than during dive. Therefore, thermal NH_4NO_3 decomposition should have increased during the cruise at 3900 m and should have been more efficient during climb compared to dive. In the light of this hypothesis, the increase of HNO_3 from about 5 to 8 nmol/mol, during the cruise at 3900 m, would indicate an NH_4NO_3 mole fraction of 3 nmol/mol. This is approximately consistent with the expected 2.75 nmol/mol of NH_4NO_3 (see below). At 3900 m, a sampling line temperature of only about 10 K larger than the ambient atmospheric temperature would have been sufficient to induce virtually complete thermal decomposition of NH_4NO_3.

It is at least conceivable that the larger NO and CO observed during climb (compared to dive) may also be related to sampling line processes. This issue needs further investigations.

Molar ratios dX/dCO_2 of excess trace substance X and excess CO_2 (excess means measured value minus atmospheric background value), measured at 3900 m the MT-plume, are given in Table 1. Also given is the mass ratio $d\mathrm{TPM}/dCO_2$ (here TPM denotes total particle matter). Furthermore, for comparison, the corresponding published emission ratios for savanna fires are also given.

ACPD
10, 7699–7743, 2010

Concerning CO, about 68% of the mean expected CO have been observed. However, when considering the range of the expected ratio of CO and CO_2 emission factors, the observed CO would represent about 49–105% of the expected CO. The missing CO may have been removed by reaction with OH (see below). Considering a reaction rate coefficient of 1.3×10^{-13} cm^3/s, a CO-depletion of 32% would imply $tp\times$(OH)eff=3.0×10^{12} scm^{-3} (range: 0–5.5×10^{12} scm^{-3}). Here tp is the plume age and (OH)eff is the effective mean OH-concentration. For a plume age of 10 days (see above), this would imply an (OH)eff of about 3.5×10^6 cm^{-3} (range: 0–6.4×10^6 cm^{-3}).

Concerning SO_2, 68% (range: 45–125%) of the expected SO_2 have been observed. The missing SO_2 may have been removed by reaction with OH and perhaps also by cloud-processes. Considering only loss by OH-reaction (reaction rate coefficient of 1.5×10^{-12} cm^3/s), one calculates $tp\times$(OH)eff=2.6×10^{11} scm^{-3} (range: 0–5.3×10^{11} scm^{-3}). Considering tp =10 days, one obtains (OH)eff=3.0×10^5 cm^{-3} (range: 0–6.2×10^5 cm^{-3}). The relatively low (OH)eff may reflect an underestimation of the SO_2 emission factor. Alternatively it may reflect reduced OH due to increased NO_x and attenuation of solar UV-radiation (see below).

Concerning NO_y, only about 17% (range 11–46%) of the expected NO_y have been observed. The missing NO_y may have experienced HNO_3-loss by cloud processes and deposition.

Concerning HNO_3, the measured HNO_3 represents 63–112% of the measured NO_y. Since NO_y is approximately equal to the sum (HNO_3+NO_x+NH_4NO_3+PAN), an upper limit to the NH_4NO_3 mole fraction of about 2.5 nmol/mol can be inferred from our measured NO_y (8.0 nmol/mol), HNO_3 (minimum: 5 nmol/mol), and NO_x (0.5 nmol/mol). PAN should not have been abundant in the plume parcel, since at the prevailing temperature (up to 292 K) PAN decomposes thermally within only about 2.7 h.

Concerning the TPM concentration at 3900 m altitude, our inferred value of 6.5×10^{-11} g/cm^3 (see above) implies a ratio $dTPM/dCO_2=4.2\times10^{-3}$ g/g. Considering the above estimated NH_4NO_3 mole fraction of about 2.5 nmol/mol, the expected NH_4NO_3-mass concentration is about 5.9×10^{-12} g/cm^3. The ratio of the emission

ACPD
10, 7699–7743, 2010

factors for primary smoke particles and CO_2 is 5.1×10^{-3} g/g. Hence it seems that the measured TPM (minus the condensed-phase NH_4NO_3) concentration represents about 74% of the expected primary TPM concentration. Therefore, it seems that loss of smoke particles by deposition and cloud-processes was not severe.

Concerning HCOH, the observed HCOH must be of secondary origin since, in clear sky conditions, HCOH is rapidly lost by photolysis. The 1/e-lifetime is only about 3 h, which is much smaller than the plume age. For example, HCOH can be formed by O_2-reaction of the PA-radical.

The UT-plume was probably uplifted by wet convection in the north-western Democratic Republic of Congo and the Central African Republic about 10 days prior to our measurements. This contrasts the transport of the MT-plume, which was uplifted south of the equator between 10 and 23 degrees south, where wet convection is much less probable and much less intense (see Real et al., 2009).

Regarding SO_2, 14–38% of the expected SO_2 have been observed, which is smaller compared to the MT-plume (45–125%). This may indicate that some of the released SO_2 experienced loss by cloud processes.

The observed HNO_3 represents only about 3.4% of the expected NO_y. However, at the much lower temperature of the UT-plume, PAN is thermally stable and may contribute about half of the NO_y while HNO_3 may contribute the other half. If so, about 6.8% of the expected HNO_3 would have been present. Compared to the lower plume (mean: 17%), this fraction of residing NO_y is still markedly smaller. This suggests more efficient HNO_3 removal by wet cloud-processes. This is, at least qualitatively, consistent with the above mentioned wet convection induced uplift of the UT-plume.

Regarding aerosol particles, dN4 and dN4(nv) are similar, which indicates that the enhanced particles contain mostly non-volatile smoke particle cores and are not new particles formed in the UT by nucleation. This is at least qualitatively consistent with the relatively low total SO_2 (80 pmol/mol), which hardly allows sufficient H_2SO_4 formation required for H_2SO_4-H_2O nucleation (see for example Fiedler et al., 2009a).

ACPD
10, 7699–7743, 2010

5 Activation potential of H_2SO_4 and NH_4NO_3 containing smoke particles

The critical (minimum) WSS required for smoke particle activation (WSSa) decreases with increasing smoke particle diameter and increasing mass fraction of soluble material contained in the smoke particle (see Fig. 12) . Conceivable smoke particle components, which are particularly efficient in this regard, are the secondary species H_2SO_4 and NH_4NO_3. The hygroscopicity of the semi-volatile organic coating of primary smoke particles is not well known. This organic coating may contain water soluble species as for example salts of organic acids. Organic acids may have experienced conversion to salts by reaction with primary pyrogenic NH_3. However, it is also conceivable that much of the organic coating is hydrophobic.

Sulfuric acid is formed in the plume via OH-induced conversion of SO_2 (see above). The 1/e-lifetime of SO_2 is determined by the OH-concentration which can be quite variable and is difficult to predict, particularly for the MT-plume where attenuation of solar UV-radiation and complex organic chemistry complicate modeling of OH. If particles and SO_2 would not be removed at different rates, the ratio of the sulfur mass concentration and primary particle mass concentration would remain equal to the ratio of the corresponding mass emission factors (mean value: 0.175/8.3=0.021) g S/g PSP; PSP denotes primary smoke particles). If the released SO_2 would ultimately be completely converted to H_2SO_4, the ratio of the H_2SO_4-mass concentration and primary smoke particle mass concentration would be about 0.065 g H_2SO_4/g PSP. Considering the ranges of expected emission factors for SO_2 and TPM, one obtains an ultimate ratio ranging from 0.025 to 0.153 g H_2SO_4/g PSP.

Our measurements made on 13 August in the MT-plume at 3900 m altitude indicate that at least 45% of the expected mean initial SO_2 were still present. Considering a measured SO_2 mole fraction of 1.4 nmol/mol (corresponding to 2.3×10^{10} SO_2 molecules cm^{-3}), this implies for 13 August at 3900 m in the MT-plume, an H_2SO_4 concentration of up to 2.8×10^{10} cm^{-3} corresponding to an H_2SO_4-mass concentration of 4.6×10^{-12} g/cm^3. Hence, if the dry particles (experimental TPM concentration:

ACPD
10, 7699–7743, 2010

6.5×10^{-11} g/cm^3) were primary smoke particles coated with secondary H_2SO_4, they would have had an approximate H_2SO_4-mass fraction of 0.071 or 7.1%. Since H_2SO_4 undergoes binary condensation, water molecules are associated with the aerosol-phase H_2SO_4.

Nitric acid is formed in the plume by OH-induced conversion of NO_2. This conversion has an effective 1/e time scale of only about 2.3 days and is about 3.3 times faster than SO_2 conversion. Hence, HNO_3 was formed first and may have converted NH_3 and ammonium salts to NH_4NO_3. However, NH_4NO_3 became thermally stable only after sufficient adiabatic cooling of the plume, after it had ascended to about 3900 m, on 8 August. At 3900 m (p =630 hPa, T =292 K, RH=25%). Here, NH_4NO_3 particles should be solid and the NH_4NO_3 dissociation equilibrium constant is about 17.6 nmol/mol×nmol/mol (for an atmospheric pressure of 630 hPa at 3900 m). This implies that the equilibrium mole fractions for each HNO_3 and NH_3 are about 4.2 nmol/mol. In comparison, expected mole fractions are <8 nmol/mol (HNO_3) (upper limit set by measured NO_y) and 12.5 nmol/mol (NH_3) (calculated from the measured dCO_2 and emission ratio NH_3/CO_2). Here, NH_3 loss by deposition and cloud processes has been neglected. Both above HNO_3 and NH_3 markedly exceed the corresponding equilibrium values. This implies that up to about 8–4.2=3.8 nmol/mol HNO_3 and 3.8 nmol/mol NH_3 would have been converted to particle-phase NH_4NO_3. The remaining 8.7 nmol/mol NH_3 would be more than sufficient to convert the H_2SO_4 to $(NH_4)_2SO_4$.

The above NH_4NO_3 mole fraction of about 2.5 nmol/mol inferred from our measurements, corresponds to about 4.0×10^{10} NH_4NO_3 molecules cm^{-3} or 5.4×10^{-12} g NH_4NO_3 cm^{-3}. Hence, mass concentrations (in g cm^{-3}) of dry smoke particle components are: 6.5×10^{-11} (total), 5.76×10^{-11} (EC+OC), 4.6×10^{-12} (H_2SO_4), and 5.4×10^{-12} (NH_4NO_3). Hence, mass fractions of dry smoke particle components are 7.07% (H_2SO_4), 8.3% (NH_4NO_3), and 15.4% (H_2SO_4+NH_4NO_3). If this soluble material (NH_4NO_3 plus H_2SO_4) would have the same decreasing effect on WSSa as NH_4NO_3, WSSa would be lowered to about 0.05%, for a smoke particle with a diameter

ACPD
10, 7699–7743, 2010

of 480 nm initially not containing soluble material (see Fig. 12).

Hence, it seems that in the MT-plume, smoke particle processing by H_2SO_4 and NH_4NO_3 may have had a marked effect on the smoke particle activation potential. It also seems that, in the aged MT-plume on 19 August, H_2SO_4 was more important than NH_4NO_3 in increasing the activation potential of smoke particles.

To investigate the evolution between 4 and 24 August, of the smoke particle size, number concentration, H_2SO_4-mass fraction, and WSSa, we have made model (AEROFOR model, Pirjola, 1999; Pirjola and Kulmala, 2001; Pirjola et al., 2003) simulations. The model assumes smoke particles with an initial uniform diameter of 125 nm and an initial number concentration of 2.2×10^5 cm^{-3}. This number concentration was calculated considering an expected $d\mathrm{TPM}/d\mathrm{CO_2}=5.1\times10^{-3}$ g/g, a $d\mathrm{TPM}=6.5\times10^{-11}$ gcm^{-3} measured on 13 August in the MT-plume at 3900 m, and an initial dTPM calculated from the measured dTPM , a specific weight of 1 g cm^{-3}, and taking an 1/e-time of 6.4 days for plume dilution. This dilution time was taken from Real et al. (2009). The plume parcel trajectory and meteorological data were taken from the LAGRANTO model. The trajectory is composed of two segments, a back-trajectory segment (4–13 August) and a forward-trajectory segment (13–24 August).

The model treats the following processes: mutual smoke particle coagulation (coagulation with entrained background particles is neglected); OH-induced SO_2-conversion to H_2SO_4; uptake of H_2SO_4 (plus associated H_2O) by smoke particles. The model is tuned to reproduce the SO_2 concentration (1.4 nmol/mol) measured on 13 August at 3900 m. Uptake of H_2SO_4 and sulfate entrained into the plume from the background atmosphere is neglected. For the period 4–13 August, the (OH)eff $=6.2\times10^5$ cm^{-3}, inferred from the observation on 13 August (at 3900 m), of 45% of the expected maximum SO_2 (see above) was considered. The corresponding noon-time OH is about 2.0×10^6 cm^{-3}. For the period tp =0–24 d (13–24 August), OH was taken from Logan et al. (1981).

ACPD
10, 7699–7743, 2010

Figure 13a shows, for the entire simulation period of 20 days (4–24 August), time sequences of the atmospheric pressure and pressure altitude of the air parcel intercepted by the Falcon on 13 August at 3900 m.

Figure 13b shows the same as Fig. 13a, but for T and RH. T varies between about 275 and 297 K. The T measured aboard the Falcon (290 K; also shown) markedly exceeds the modeled value (280 K). This discrepancy may be due to additional heating via light absorption by soot containing smoke particles. RH varies between about 8 and 50%. The largest local maxima of about 50% are reached during the initial ascend at tp =2 d and during the final ascend at tp =20 d. Water vapor supersaturation (RH>100%), according to the model, was never reached.

Figure 14 shows time sequences of the modeled molecular number concentrations of OH, SO_2, and gas-phase H_2SO_4. Also given is a curve representing an inert plume dilution tracer having the same initial concentration as SO_2. Both, OH and gas-phase H_2SO_4 exhibit a pronounced diurnal variation. The SO_2 concentration curve exhibits a weak diurnal variation and decreases with time much more steeply than the plume dilution tracer. This indicates that SO_2-depletion was preferably due to OH-induced SO_2-conversion to gas-phase H_2SO_4.

Figure 15a shows a time sequence of number concentrations Nsp of smoke particles in the plume parcel. Nsp decreases with increasing plume age tp, due to coagulation and plume dilution. Initially coagulation dominates and later, as Nsp has decreased sufficiently, coagulation becomes slow and plume dilution dominates. For tp =10 days (13 August), the model Nsp is 1000 cm^{-3}, which is smaller than measured Nsp (2000 cm^{-3}). After 20 days, Nsp has decreased to about 200 cm^{-3}.

Figure 15b shows a time sequence of the smoke particle diameter Dsp for two cases: without and with binary H_2SO_4-H_2O condensation. Without binary H_2SO_4-H_2O condensation, Dsp increases to 450 nm (tp =10 d) and 470 nm (20 d), due to mutual smoke particle coagulation. With binary H_2SO_4-H_2O condensation, as tp increases, Dsp increases to 490 nm (tp =10 d) and 545 nm (20 d), due to mutual smoke particle coagulation plus binary H_2SO_4-condensation. For tp =10 d (13 August), the modeled

ACPD
10, 7699–7743, 2010

Dsp=450 nm (without binary H_2SO_4-H_2O condensation) is close to the peak dry Dsp (about 400 nm) of the experimental aerosol volume size distribution.

Figure 16a shows a time sequence of the mass concentrations of the primary smoke particle components (EC+OC), and the secondary components H_2SO_4, and H_2O. The EC+OC curve decreases by a factor of about 20, due to plume dilution. On day 1, the H_2SO_4 curve increases steeply and on days 3–6 reaches a maximum of about 6000 ng/m^3. Hereafter until tp =13 d the H_2SO_4 curve decreases only moderately, and ultimately it decreases more steeply. The H_2O mass fraction of smoke particles varies, mostly in response to the variability of RH.

Figure 16b shows a time sequence of the H_2SO_4-mass fraction of smoke particles. It exhibits a slight diurnal variation but generally increases throughout the simulation period. At tp =10 d (13 August) it is about 9% and at tp =24 d (24 August) it is about 14%.

Modeled WSSa as function of modeled diameters and H_2SO_4-mass fractions of smoke particles, for four tp (1, 2, 4, 6, 10, 24 days) are given in Fig. 12. Here it is assumed that H_2SO_4 has the same effect on WSSa as NH_4NO_3 (for which the figure was originally plotted, see Seinfeld and Pandis, 1998). Hence, if the only soluble material contained in the smoke particles would be H_2SO_4, WSSa would decrease with tp from about 0.3% (tp =1 d) to about 0.033% (t =24 d). Also included are values for the sum mass fraction of H_2SO_4 and NH_4NO_3. Now WSSa decreases to about 0.025% (tp =24 d).

In comparison, WSS involved in maritime cloud formation are about 0.3–0.8% (cumulus clouds) and about 0.05% (maritime stratiform clouds). Hence, H_2SO_4-processed smoke particles contained in the plume parcel under consideration have developed a potential for maritime cumulus cloud formation (after 1 day) and for maritime stratiform cloud formation (after 10 days).

However, the modeled RH (Fig. 13b) never exceeded 100% in the plume parcel under consideration. It is conceivable that small fluctuations, which are not considered by the model, may have resulted in small WSS, particularly at tp when the modeled

CC BY

RH was large (tp =2 and 24 d).

6 Summary and conclusions

The main findings of the reported airborne BMB plume measurements are:

(a) Two aged BB plumes, located at about 10 800–11 200 m and 3000–5500 m altitude, have been probed above the eastern Atlantic (Gulf of Guinea).

(b) The plumes originated from BB fires in the Southern Hemisphere African savanna belt.

(c) The lower, much more polluted plume had greatly elevated abundances of gas-phase and particle-phase pollutants.

(d) The gases SO_2 (precursor of H_2SO_4) and HNO_3, which have a potential to mediate smoke particle activation had measured mole fractions of up to 1400 and 9000 pmol/mol.

(e) Our data indicate that a large part of NO_y experienced loss via HNO_3 by cloud-processes and possibly also by deposition.

(f) SO_2 did not experience marked loss by deposition and cloud-processes.

(g) As the lower plume was ageing and diluting, SO_2 experienced OH-induced conversion to H_2SO_4, which experienced rapid binary (H_2SO_4-H_2O)-condensation on smoke particles.

(h) H_2SO_4 condensation, besides coagulation size growth, increased the activation potential of smoke particles. Also NH_4NO_3 formation contributed somewhat to increase the activation potential.

ACPD
10, 7699–7743, 2010

(i) After 13 August (day of our measurements), the lower plume traveled over the Atlantic while descending to 1300 m altitude after 8 days. On 19 August it reached the west coast of south America (French Guyana) and hereafter traveled northward over the Atlantic.

(j) On 19 August, smoke particles had a potential to become activated already at a very small WSS of only 0.05%, which would allow them to act as CCN in maritime stratiform cloud formation.

Acknowledgements. Based on a French initiative, AMMA was built by an international scientific group and is currently funded by a large number of agencies, especially from France, UK, US and Africa. It has been the beneficiary of a major financial contribution from the European Community's Sixth Framework Research Programme. Detailed information on scientific coordination and funding is available on the AMMA International web site http://www.amma-international.org. We are furthermore grateful to the crew of the DLR Flight Department for their commitment and support to collect this data set. We also thank our colleagues Michael Lichtenstern, Paul Stock, Anke Roiger (DLR) and Bernhard Preissler, Ralph Zilly (MPI-K) for their support in instrument operation. This work was funded by DLR, MPI-K and Metropolia University of Applied Sciences, Helsinki.

The service charges for this open access publication have been covered by the Max Planck Society.

References

Andreae, M.: Soot carbon and excess fine potassium: Long-range transport of combustion-derived aerosols, Science, 220, 1148–1151, 1983. 7701

Andreae, M.: Biomass burning: Its history, use, and distribution and its impact on environmental quality and global climate, in: Global biomass burning: Atmospheric, climatic, and biospheric implications, MIT press, Cambridge, MA, London, 3–21, 1991. 7701

Andreae, M. and Merlet, P.: Emission of trace gases and aerosols from biomass burning, Global Biogeochem. Cy., 15, 955–966, 2001. 7701, 7726

Crutzen, P. and Andreae, M.: Biomass burning in the tropics: Impact on atmospheric chemistry and biogeochemical cycles, Science, 250, 1669–1678, 1990. 7701

Crutzen, P., Heidt, L., Krasnec, J., Pollock, W., and Seiler, W.: Biomass burning as a source of atmospheric gases CO, H_2, N_2O, CH_3Cl and COS, Nature, 282, 253–256, 1979. 7701

Fiedler, V., Arnold, F., Schlager, H., Drnbrack, A., Pirjola, L., and Stohl, A.: East Asian SO_2 pollution plume over Europe – Part 2: Evolution and potential impact, Atmos. Chem. Phys., 9, 4729–4745, 2009a, http://www.atmos-chem-phys.net/9/4729/2009/. 7705, 7715

Fiedler, V., Nau, R., Ludmann, S., Arnold, F., Schlager, H., and Stohl, A.: East Asian SO_2 pollution plume over Europe – Part 1: Airborne trace gas measurements and source identification by particle dispersion model simulations, Atmos. Chem. Phys., 9, 4717–4728, 2009b, http://www.atmos-chem-phys.net/9/4717/2009/. 7705

Folkins, I., Wennberg, P., Hanisco, T., Anderson, J., and Salawitch, R.: OH, HO_2, and NO in two biomass burning plumes: Sources of HO_x and implications for ozone production, Geophys. Res. Lett., 24, 3185–3188, 1997. 7704

Gerbig, C., Schmitgen, S., Kley, D., Volz-Thomas, A., Dewey, K., and Haaks, D.: An improved fast-response vacuum-UV resonance fluorescence CO instrument, J. Geophys. Res., 104, 1699–1704, 1999. 7705, 7727

Houghton, J. T., Ding, Y., Griggs, D., and et al.: Intergovernmental Panel on Climate Change (IPCC): Climate Change 2001, Cambridge Univ. press, 2001. 7701

Koppmann, R., von Czapiewski, K., and Reid, J. S.: A review of biomass burning emissions, part I: gaseous emissions of carbon monoxide, methane, volatile organic compounds, and nitrogen containing compounds, Atmos. Chem. Phys. Discuss., 5, 10455–10516, 2005, http://www.atmos-chem-phys-discuss.net/5/10455/2005/. 7701

Kormann, R., Fischer, H., de Reus, M., Lawrence, M., Brühl, Ch., von Kuhlmann, R., Holzinger, R., Williams, J., Lelieveld, J., Warneke, C., de Gouw, J., Heland, J., Ziereis, H., and Schlager, H.: Formaldehyde over the eastern Mediterranean during MINOS: Comparison of airborne in-situ measurements with 3-D-model results, Atmos. Chem. Phys., 3, 851–861, 2003, http://www.atmos-chem-phys.net/3/851/2003/. 7706, 7727

Logan, J., Prather, M., Wofsy, S., and McElroy, M.: Tropospheric Chemistry: A Global Perspective, J. Geophys. Res., 86, 7210–7254, 1981. 7718

Pirjola, L.: Effects of the increased UV radiation and biogenic VOC emissions on ultrafine aerosol formation, J. Aerosol Sci., 30, 355–367, 1999. 7718

Pirjola, L. and Kulmala, M.: Development of particle size and composition distribution with a novel aerosol dynamics model, Tellus, 53B, 491–509, 2001. 7718

Pirjola, L., Tsyro, S., Tarrason, L., and Kulmala, M.: A monodisperse aerosol dynamics module – a promising candidate for use in the Eulerian long-range transport model, J. Geophys. Res., 108, 4258, doi:10.1029/2002JD002867, 2003. 7718

Real, E., Orlandi, E., Law, K. S., Fierli, F., Josset, D., Cairo, F., Schlager, H., Borrmann, S., Kunkel, D., Volk, M., McQuaid, J. B., Stewart, D. J., Lee, J., Lewis, A., Hopkins, J. R., Ravegnani, F., Ulanovski, A., and Liousse, C.: Cross-hemispheric transport of central African biomass burning pollutants: implications for downwind ozone production, Atmos. Chem. Phys. Discuss., 9, 17385–17427, 2009, http://www.atmos-chem-phys-discuss.net/9/17385/2009/. 7701, 7715, 7718

Reid, J. S., Eck, T. F., Christopher, S. A., Koppmann, R., Dubovik, O., Eleuterio, D. P., Holben, B. N., Reid, E. A., and Zhang, J.: A review of biomass burning emissions part III: intensive optical properties of biomass burning particles, Atmos. Chem. Phys., 5, 827–849, 2005, http://www.atmos-chem-phys.net/5/827/2005/. 7701, 7711

Reiner, T. and Arnold, F.: Laboratory flow reactor measurements of the reaction $SO_3 + H_2O + M \rightarrow H_2SO_4 + M$: Implications for gaseous H_2SO_4 and aerosol formation in the plume of jet aircraft, Geophys. Res. Lett., 20, 2659–2662, 1993. 7702

Reiner, T. and Arnold, F.: Laboratory investigations of gaseous sulfuric acid formation via $SO_3+H_2O+M \rightarrow H_2SO_4+M$: Measurements of the rate constant and products identification, J. Chem. Phys., 101, 7399–7407, 1994. 7702

Schlager, H., Konopka, P., Schulte, P., Schumann, U., Ziereis, H., Arnold, F., Klemm, M., Hagen, D. E., Whitefield, P. D., and Ovarlez, J.: In situ observations of air traffic emission signatures in the North Atlantic flight corridor, J. Geophys. Res., 102, 10739–10750, 1997. 7706, 7727

Schulte, P., Schlager, H., Ziereis, H., Schumann, U., Baughcum, S., and Deidewig, F.: NO_x emission indices of subsonic long-range jet aircraft at cruise altitude: In situ measurements and predictions, J. Geophys. Res., 102, 21431–21442, 1997. 7706, 7727

Seinfeld, J. and Pandis, S.: Atmospheric Chemistry and Physics, John Wiley & Sons, Inc., first edn., 1998. 7702, 7703, 7720, 7739

Singh, H., O'Hara, D., Herlth, D., Sachse, G., Blake, D., Bradshaw, J., Kanakidou, M., and Crutzen, P.: Acetone in the atmosphere: Distribution, sources, and sinks, J. Geophys. Res., 99, 1805–1819, 1994. 7704

Speidel, M., Nau, R., Arnold, F., Schlager, H., and Stohl, A.: Sulfur dioxide measurements in the

lower, middle and upper troposphere: Deployment of an aircraft-based chemical ionization mass spectrometer with permanent in-flight calibration, Atmos. Environ., 41, 2427–2437, 2007. 7705, 7727

Wernli, H. and Davies, H.: A Lagrangian-based analysis of extratropical cyclones. I: The method and some applications, Q. J. R. Meteorol. Soc., 123, 467–489, 1997. 7708

Ziereis, H., Schlager, H., Schulte, P., van Velthoven, P., and Slemr, F.: Distributions of NO, NOx, and NOy in the upper troposphere and lower stratosphere between 28° and 61° N during POLINAT 2, J. Geophys. Res., 105, 3653–3664, 2000. 7706, 7727

Table 1. Emission factors Ex, molar emission ratios Ex/ECO_2 and the measured excess molar emission ratio dx/dCO_2(adopted from Andreae and Merlet, 2001).

Substance x	Ex (g/kg)	Ex/ECO_2 (mol/mol)	dx/dCO_2 (mol/mol)	R
CO	65±20	$6.3\times10^{-2}\pm2.2\times10^{-2}$	4.3×10^{-2}	6.8×10^{-1}
TPM	8.3	5.1×10^{-3} g/g	$>2.5\times10^{-3}$ g/g	$>4.9\times10^{-1}$
NO_y	3.9±2.2	$3.5\times10^{-3}\pm2.2\times10^{-3}$	6×10^{-4}	1.7×10^{-1}
NO_x	–	–	3.8×10^{-5}	–
PAN	–	–	9.2×10^{-5}	–
HNO_3	–	–	$3.8\text{-}6.9\times10^{-4}$	–
NH_3	0.6-1.5	$1.0\text{-}2.4\times10^{-3}$	$<1\times10^{-4}$	$<1\times10^{-1}$
SO_2	0.35± 16	$1.5\times10^{-4}\pm0.7\times10^{-4}$	1×10^{-4}	6.7×10^{-1}
HCHO	0.26-0.44	$2.3\text{-}4.0\times10^{-4}$	7.7×10^{-5}	$3.3\text{-}1.9\times10^{-1}$
CO_2	1613	–	$dCO_2=1.3\times10^{-5}$	–

ACPD
10, 7699–7743, 2010

Table 2. Compilation of instruments deployed on the Falcon during AMMA. Also compiled are detection limits and uncertainties.

Substance	Method	Det. Limit (2σ) [nmol/mol]	Time resolution [s]	Accuracy [%]	Reference
SO_2	CIMS	0.02	1	12	Speidel et al. (2007)
HNO_3	CIMS	?	1	?	this paper
NO	Chemiluminescence	0.005	1	8	Schlager et al. (1997)
NO_y	Chemiluminescence	0.015	1	15	Ziereis et al. (2000)
CO	Fluorescence	3	5	10	Gerbig et al. (1999)
CO_2	NDIR	100	1	0.1	Schulte et al. (1997)
H_2CO	Hantzsch reaction	0.084	180	30	Kormann et al. (2003)
O_3	UV absorption	1	4	5	Schlager et al. (1997)

ACPD
10, 7699–7743, 2010

(a)

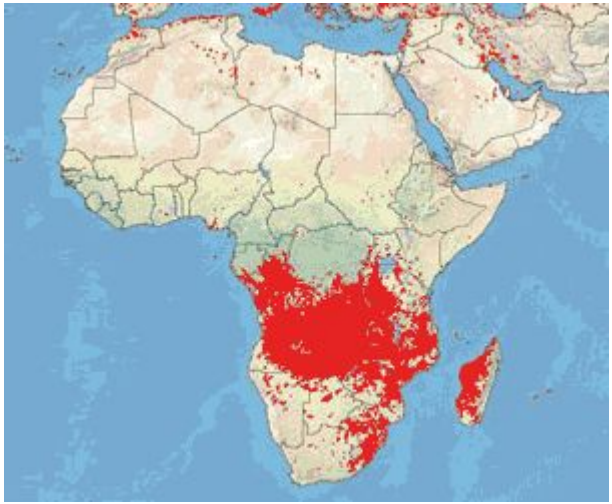

(b)

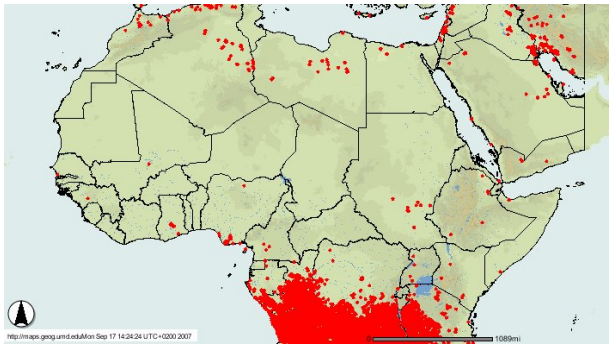

Fig. 1. Fires in Central Africa detected by MODIS (see text) for **(a)** Africa in August 2006 and **(b)** Northern Africa between the 1st and the 10 August 2006.

ACPD

10, 7699–7743, 2010

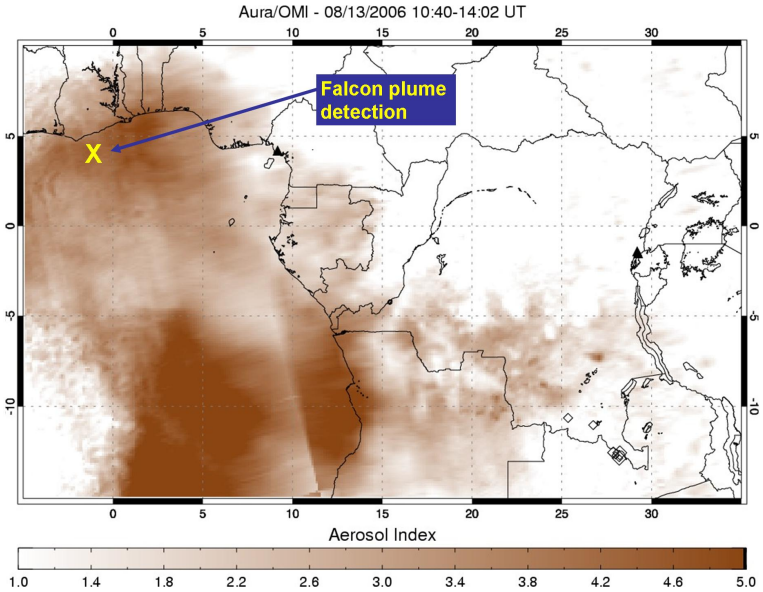

Fig. 2. Aerosol Index AI of light absorbing aerosols measured by OMI on Satellite AURA on the 13 August 2006.

ACPD
10, 7699–7743, 2010

CC BY

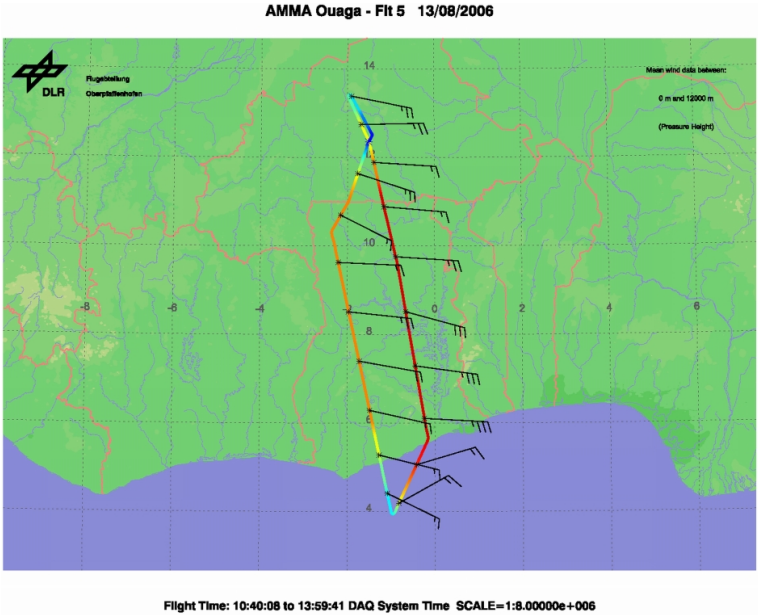

Fig. 3. Flight path of the research aircraft Falcon (AMMA flight 20060813). The colors from blue to red roughly indicate the altitude (0–11 km). Distance of the wind direction markers is 10 min, 1° Longitude corresponds to approximately 110 km, 1° Latitude to 111 km.

ACPD
10, 7699–7743, 2010

CC BY

(a)

(b)

Fig. 4. Photographs taken by one of the coauthors aboard the Falcon at an altitude of 5500 m just above the pollution plume **(a)** and at 3900 m inside the plume **(b)**.

ACPD

10, 7699–7743, 2010

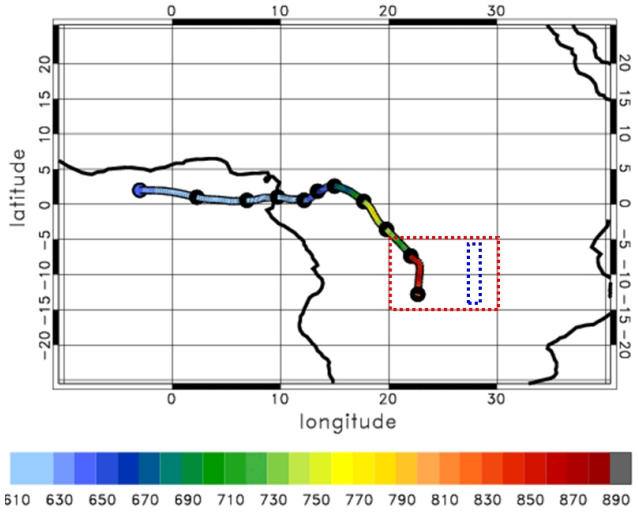

Fig. 5. LAGRANTO 10-day back-trajectory starting at 13 August 2006 12:00 UTC. The color bar gives the air trajectory pressure. The red dots mark the core fire region as shown in Fig. 1 and the blue dots mark the so-called African copper belt.

ACPD
10, 7699–7743, 2010

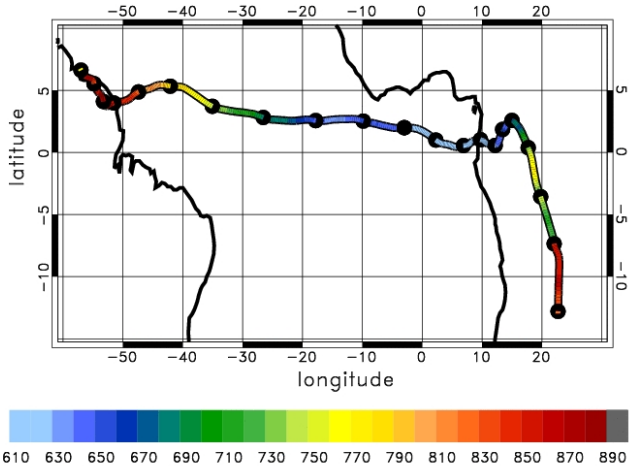

Fig. 6. Combination of the LAGRANTO 10-day back-trajectory with a LAGRANTO 10-day forward simulation starting on 13 August 12:00 UTC. The color bar gives the air trajectory pressure.

ACPD
10, 7699–7743, 2010

(a)

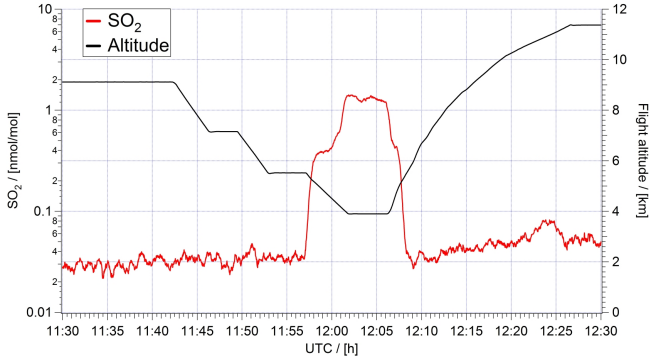

(b)

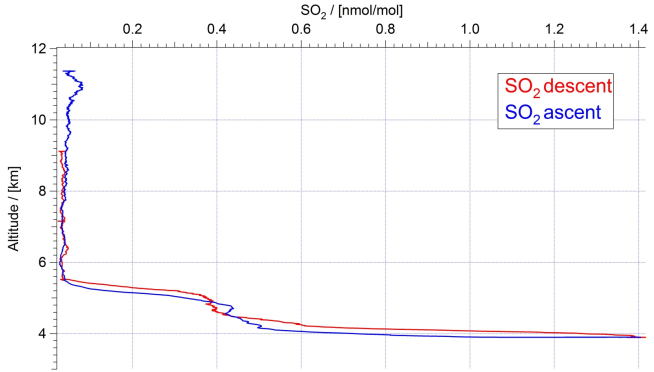

Fig. 7. **(a)** Timeseries of the measured SO_2 mole fraction and the Falcon flight altitude, **(b)** altitude profile of the measured SO_2 mole fraction (descent in red, reascent in blue).

ACPD
10, 7699–7743, 2010

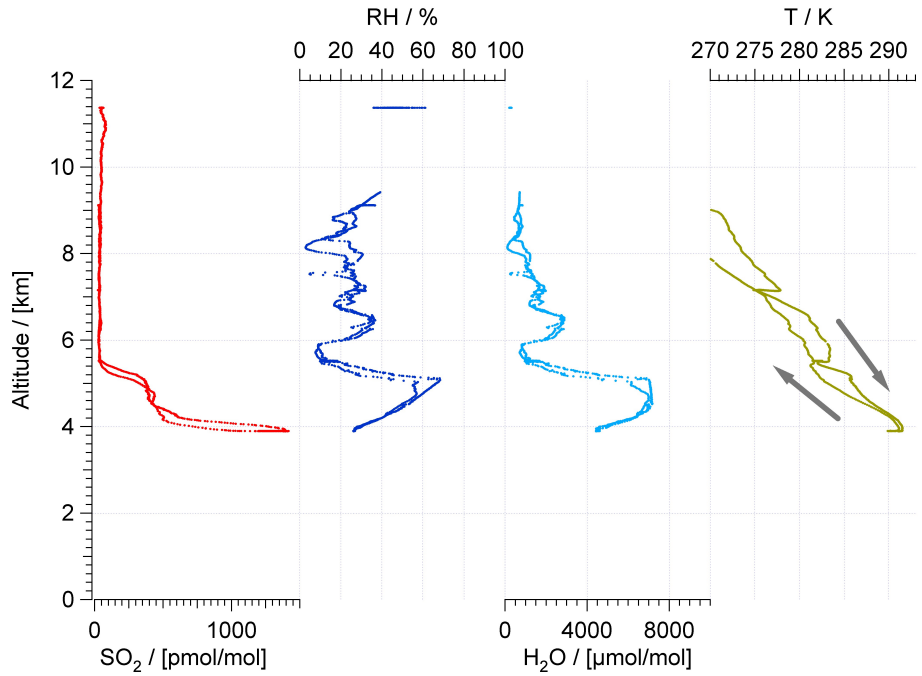

Fig. 8. Vertical profiles of SO_2 mole fraction, relative humidity, water vapor mole fraction and temperature. The arrows mark ascend and descend.

ACPD
10, 7699–7743, 2010

(a)

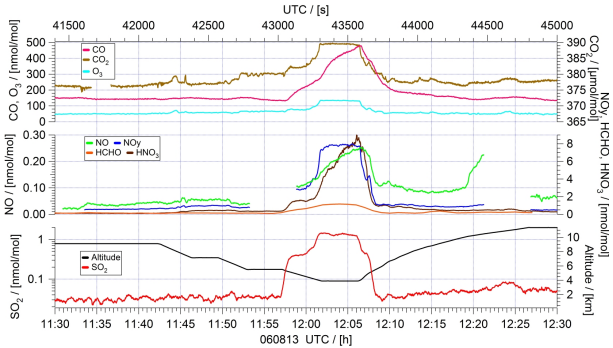

(b)

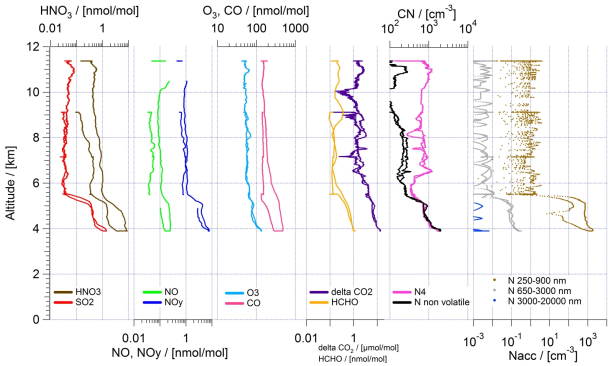

Fig. 9. (a) Time sequences of measured atmospheric trace gases. Bottom panel: SO_2 mole fraction and flight altitude. Middle Panel: NO, NO_y, H_2CO and HNO_3 mole fractions. Upper panel: CO, CO_2 and O_3 mole fractions. Between 11:57 and 12:08 UTC the pollution plume is detected in all trace gases. **(b)** Corresponding vertical profiles of measured trace gases and particles.

ACPD
10, 7699–7743, 2010

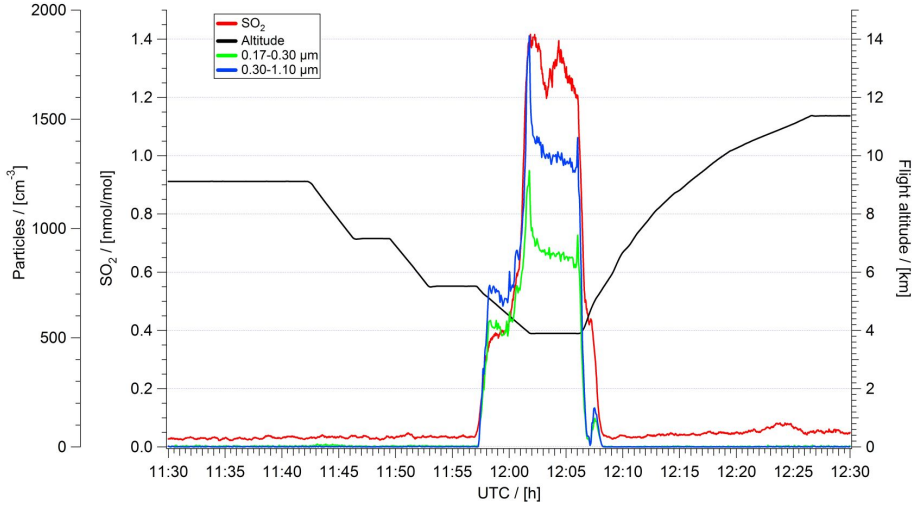

Fig. 10. Time sequences of number concentrations of aerosol particles possessing diameters from 170 to 300 nm and from 300 to 1100 nm. Also given are time sequences of the SO_2 mole fraction and the flight altitude of the Falcon.

ACPD
10, 7699–7743, 2010

CC BY

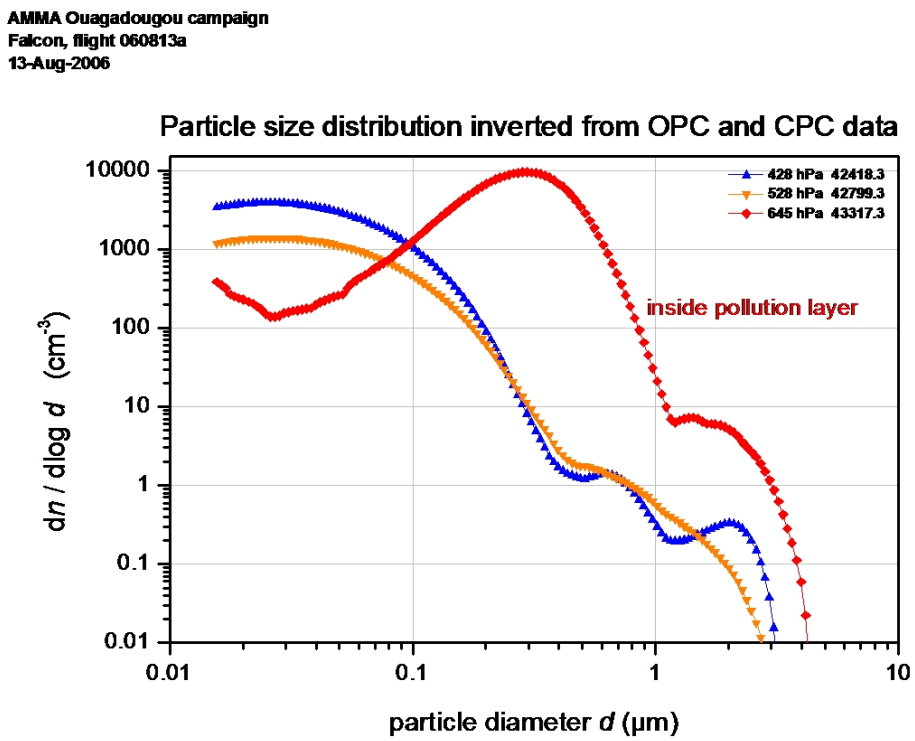

Fig. 11. Three aerosol particle size distributions measured above the MT-plume at 7000 m (428 hPa), 4500 m (528 hPa), and in the MT-plume at 3900 m (645 hPa) altitude.

ACPD
10, 7699–7743, 2010

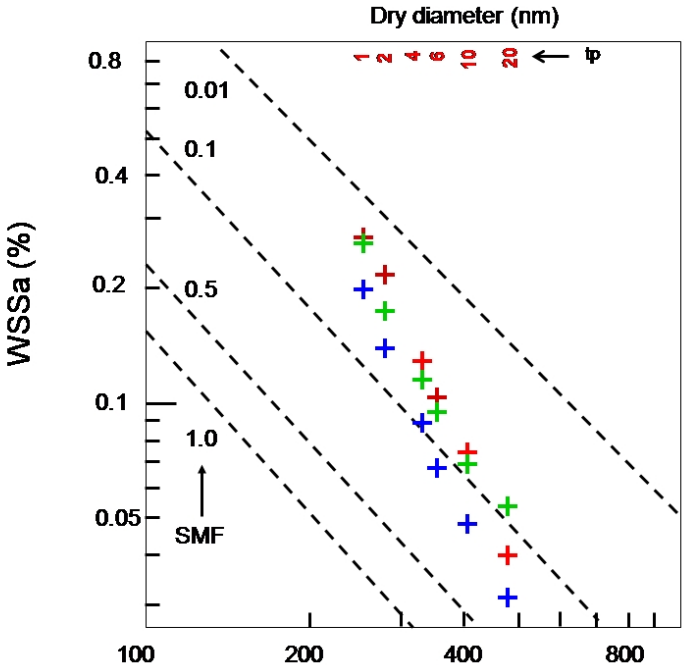

Fig. 12. Critical water vapor supersaturation WSSa as function of aerosol particle dry diameter (nm) for different NH_4NO_3 soluble mass fractions (SMF=0.01, 0.1, 0.5, 1.0) (adopted from Seinfeld and Pandis, 1998). Also given are experimental data (crosses) for the plume parcel intercepted on 13 August 2006 at 3900 m altitude, including two cases (H_2SO_4 only: red cross; H_2SO_4+NH_4NO_3: blue cross). The remaining green data points are predictions of an aerosol model for the same plume parcel, but for different plume ages (tp =1, 2, 10 and 15 days).

ACPD
10, 7699–7743, 2010

(a)

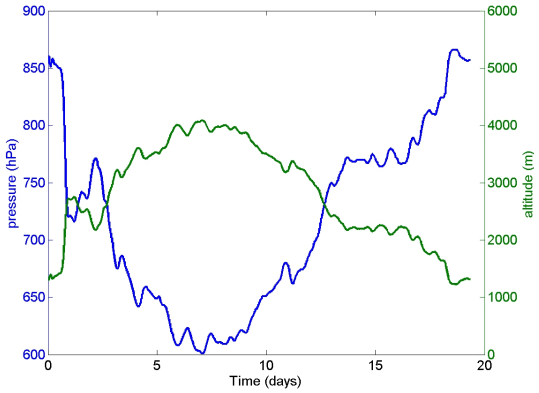

(b)

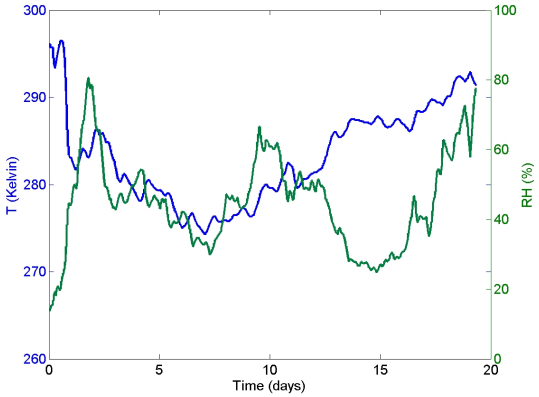

Fig. 13. (a) Time sequences of the atmospheric pressure and pressure altitude of the air parcel intercepted by the Falcon on 13 August at 3900 m for the entire simulation period of 20 days (4–24 August). **(b)** The same but for temperature and relative humidity.

ACPD
10, 7699–7743, 2010

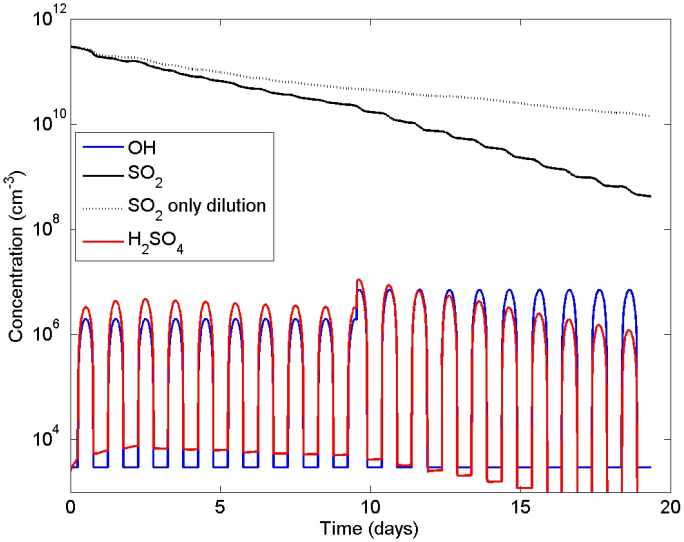

Fig. 14. Time sequences of the modeled molecular number concentrations of OH, SO_2 and gas-phase H_2SO_4. Also given is a curve representing an inert plume dilution tracer having the same initial concentration as SO_2 (SO_2 only dilution).

ACPD
10, 7699–7743, 2010

(a)

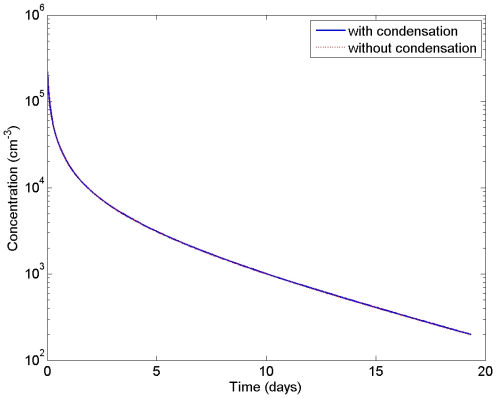

(b)

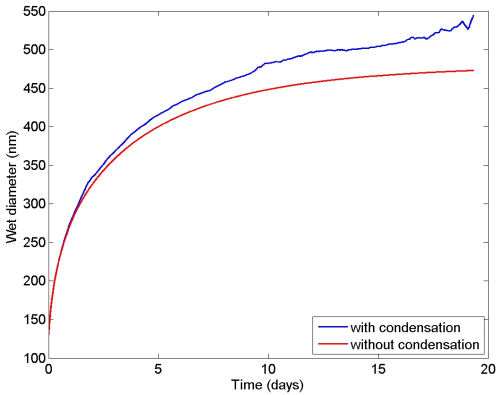

Fig. 15. (a) Time sequence of number concentrations of smoke particles in the plume parcel. **(b)** Time sequence of the smoke particle diameter Dsp for two cases: without and with binary H_2SO_4–H_2O condensation.

ACPD
10, 7699–7743, 2010

(a)

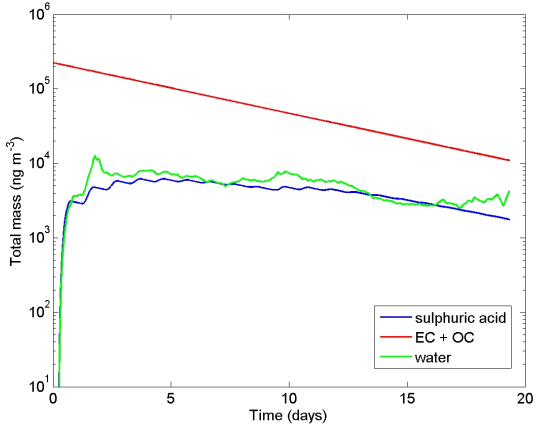

(b)

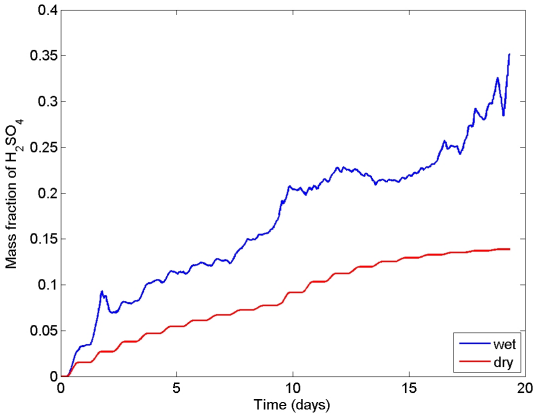

Fig. 16. (a) Time sequence of the mass concentrations of the primary smoke particle components (EC+OC), and the secondary components H_2SO_4 and H_2O. **(b)** Time sequence of the H_2SO_4 mass fraction of smoke particles.

ACPD
10, 7699–7743, 2010